Earth and Planetary Science Letters 594 (2022) 117711

Contents lists available at ScienceDirect

Earth and Planetary Science Letters

www.elsevier.com/locate/epsl

Out of sequence faulting in the backbone range, Taiwan: Implications for thickening and exhumation processes

Yuan-Hsi Lee [a,*], Timothy B. Byrne [b], Wei Lo [c], Shao-Jyun Wang [a], Shuh-Jong Tsao [d], Cheng-Hong Chen [e], Han-Cheng Yu [b], Xinbin Tan [f], Matthijs van Soest [g], Kip Hodges [g], Lucas Mesalles [a], Holden Robinson [b], Julie C. Fosdick [b]

[a] Department of Earth and Environmental Sciences, National Chung Cheng University, Taiwan
[b] Department of Earth Sciences, University of Connecticut, Storrs, CT 06269, USA
[c] Department of Materials and Mineral Resources Engineering, National Taipei University of Technology, Taiwan
[d] Central Geological Survey, MOEA, Taiwan
[e] Department of Geosciences, National Taiwan University, Taiwan
[f] Institute of Geology, China Earthquake Administration, Beijing 100029, China
[g] School for Earth and Space Exploration, Arizona State University, Tempe, AZ 85281, USA

ARTICLE INFO

Article history:
Received 30 August 2021
Received in revised form 29 June 2022
Accepted 2 July 2022
Available online xxxx
Editor: A. Webb

Keywords:
Taiwan orogenic belt
out of sequence thrust
thermochronology dates
exhumation process

ABSTRACT

The Taiwan orogenic belt results from convergence between the Philippine Sea plate and Eurasia plate since the late Cenozoic. An extremely high exhumation rate has been observed in the Backbone Range, which has motivated interpretive models that show underplating as the primary process in driving uplift and thickening. Here we integrate new (U-Th)/He and fission-track dates of detrital zircons with previously published thermochronology to document a significant out-of-sequence thrust in the core of Taiwan orogen. The thrust, informally named the Tayulin fault system, is identified by structural kinematics and offset metamorphic temperature trends, low-temperature thermochronometric dates, and seismic tomography. The OOST appears to be composed of three segments that crop out along the western flank of the Backbone Range. The apparent age-elevation profiles suggest a relatively slow exhumation rate, <1.0 mm/yr, in the early stages from 8 Ma to 2 Ma followed by a stage of significantly higher exhumation rates, ranging from 2.3 to 6.5 mm/yr after 2 Ma. The early slow exhumation stage is related to regional folding and foliation development. In contrast, we suggest the younger rapid exhumation stage is related to slip on the out-of-sequence thrust.

1. Introduction

Arc–continent collisions, like the active orogen in Taiwan, have long been recognized as integral parts of orogenic systems and are often interpreted in terms of critical wedge theory where the taper is maintained by thickening of the wedge interior (Chapple, 1978; Davis et al., 1983; Suppe, 1981). Three primary internal thickening mechanisms have been recognized: (1) penetrative strain due to slipping on a significant fault (Clark et al., 1993), (2) underplating through duplex accretion (Malavieille, 2010), and (3) faulting within the wedge, i.e., out-of-sequence thrusting (OOST), (Morley, 1988). These processes can act sequentially or contemporaneously as they stabilize the critically tapered wedge, forming one or more complex duplex structures associated with penetrative cleavages and OOSTs.

In some orogens, slip along the OOST is localized, and a single, long-lived OOST records significant displacement, separating hanging wall and footwall blocks with different mechanical properties. In modern convergent margins, these large-displacement OOSTs define inner and outer wedges that, in some cases, delineate tsunamigenic systems (Moore et al., 2007). Field studies (McQuarrie et al., 2014; Webb, 2013), ocean drilling (Moore et al., 2007), and modeling (Konstantinovskaia and Malavieille, 2005) argue that formation of large-displacement OOST reflects fundamental changes in wedge dynamics. For example, accretion of large sediment volumes, removal of previously accreted materials through erosion or tectonic exhumation, or changes in the thickness of the subduction channel can cause stress permutations resulting in large displacement OOSTs.

Critical wedge theory has been used to interpret mountain-building processes in Taiwan quantitatively (Suppe, 1981;

* Corresponding author.
E-mail address: seilee@eq.ccu.edu.tw (Y.-H. Lee).

https://doi.org/10.1016/j.epsl.2022.117711
0012-821X/

Barr and Dahlen, 1989; Clark et al., 1993; Fuller et al., 2006; Simoes et al., 2007), and most interpretations argue for penetrative deformation or underplating of materials beneath the wedge to balance accretion. For example, Barr and Dahlen (1989) suggested that at least 25% of the underthrust material needed to be underplated to explain the metamorphic grade in the eastern Backbone Range in Taiwan. Using different wedge parameters, other models suggest even higher values of underplating (e.g., 50 to 90%) to fit observed exhumation rates and metamorphic temperatures (Simoes et al., 2007; Fuller et al., 2006). Malavieille (2010) used a sandbox to model critically tapered wedges and proposed two zones of underplating in Taiwan's orogenic wedge, one beneath the Backbone Range and a second beneath the Hsüehshan Range. The underplating model predicts that duplex structures develop in the deeper parts of the wedge as the upper detachment fault is passively uplifted and folded, forming an antiformal stack of thrust sheets. These models also suggest limited development of compressional structures in the upper crust. In contrast, a recent study in southern Central Range suggested the absence of nappe stacking in the Backbone Range (Conand et al., 2020) and late-stage thrust faults have also been observed in the core of the Taiwan orogen (Lee and Yang, 1994; Tillman and Byrne, 1995), suggesting that these simple models do not fully capture the complex evolution of Taiwan orogenic wedge.

To better understand the role of late-stage structures in the core of the Taiwan orogen and the exhumation mechanism of the Backbone Range exhumation, we integrate 14 new U-Th/He (ZrnHe) and 126 new fission-track (ZrnFT) ages of detrital zircons with previously published thermochronologic data (Tsao et al., 1992, 1996; Liu et al., 2001; Hsu et al., 2016; Lee et al., 2006, 2015; Beyssac et al., 2007; Mesalles et al., 2014; Shen et al., 2020), paleotemperature (Chen and Wang, 1994; Beyssac et al., 2007; Horng et al., 2012; Conand et al., 2020), and structural data (Lu et al., 1989; Lo and Yen, 1993; Lee and Yang, 1994; Stanley et al., 1981; Tillman and Byrne, 1995) along several transects that cross the western flank of the Backbone Range of Taiwan orogen. Our results confirm the importance of late-stage deformation and indicate the presence of a significant system of out-of-sequence thrust faults in the core of the orogen, which we refer to here as the Tayulin fault system. The identified thrust system consists of three overlapping segments, or splays, that crop out along the western flank of the Backbone Range ca 270 km. The splays generally follow the topographic grain of the orogen, suggesting a relation to the topographic growth of the orogen. Below we describe evidence for the fault system, focusing on the Central and Southern Cross-Island Highways as they provide the most control on the geometry and slip of the fault, then provide a summary of data from the northern and southern extents of the fault (Fig. 1). We integrate these new observations and data sets with different interpretations of the significance of the thrust system in the growth of the orogen.

2. Geologic background

As the northern Luzon arc moves northwest at a ca. 8 cm/yr (Yu et al., 1997), it collides with the Eurasian continental margin, forming one of the planet's archetypical examples of an arc-continent collisional orogenic system. In addition to the colliding arc, exposed in the Coastal Range, the bedrock geology of the resulting orogen can be subdivided into four tectonostratigraphic units from east to west (Ho, 1986) (Fig. 1): (1) a high-pressure metamorphic belt of Miocene age, the Yuli belt (YL) (Chen et al., 2017; Keyser et al., 2015); (2) the Mesozoic Tailuko Belt of Eurasian affinity that crops out west of the Yuli Belt in the eastern Backbone Range (BR-M); (3) two slate belts, the western Backbone Range slate belt (BR-C) and the Hsüehshan Range slate belt (HR) composed of passive margin sediments, and (4) a fold-and-thrust belt exposed in the Western Foothills (WF) and composed of unmetamorphosed passive margin sedimentary rocks. (Fig. 1a).

3. Research approach

The rocks of the metamorphic core of Taiwan are exposed along the middle of the Backbone Range and, due to the steep topography and dense vegetation, most detailed structural studies have been concentrated along one of the three highways that cross the orogen. Most structural studies have also focused on regional scale lithologic variations and structural geometries (Stanley et al., 1981; Lo and Yen, 1993; Lee and Yang, 1994), with only a handful focusing on late-stage structures, including any structures that might be "out-of-sequence." To overcome the difficulty of mapping in rugged terrane and correlating mappable units between limited outcrops, we combine paleotemperature and low-temperature thermochronology data with focused structure data collected across several orogen-normal transects. The metamorphic facies map of Taiwan, based primarily on illite crystallinity (Chen and Wang, 1994), provides a general outline of the distribution of paleotemperatures, including possible out-of-sequence structures. More recently, Horng et al. (2012) showed that the occurrence of pyrrhotite, correlated with the epizone mapped by Chen and Wang (1994) and could be used as an index mineral for the greenschist facies. Their work expanded and clarified the distribution of the epizone and anchizone zones in the Slate Belt, and we use these revised zones as a general guide in locating late-stage structures. The epizone and anchizone zones are interpreted to correspond to the greenschist (GR) to prehnite-pumpellyite (PP) zones, respectively, with transition paleotemperature of ~300°C (Fig. 1a). The identified zones are also consistent with the metamorphic temperatures measured with Raman spectrum of carbonaceous material (RSCM) (Beyssac et al., 2007; Conand et al., 2020). Low-temperature thermochronologic data, primarily zircon fission track (ZrnFT) and (U-Th)/He (ZrnHe) data from detrital zircons (Beyssac et al., 2007; Hsu et al., 2016), and K/Ar ages of fine-grained white micas collected from slates and phyllites (Tsao et al., 1992, 1996), complement the paleotemperature data (Horng et al., 2012) and help constrain the age of faulting events and average slip rates.

The distribution of peak paleotemperatures in the orogen generally follows stratigraphic patterns, with older sedimentary units recording higher paleotemperatures (Chen and Wang, 1994). Older stratigraphic sequences, however, generally lie structurally above younger units, suggesting inversion during accretion and collision. When this inversion occurred and what structures accommodated the over-turning, which, in part, motivated the current research.

We focus here on the eastern portion of the Slate Belt exposed in the Backbone Range and western parts of the Tailuko Belt near the Slate Belt. We start with the description of structures and paleotemperature and low-temperature geochronologic data from the two, east-west trending highways as these areas provide the most data across the proposed fault. Previous field studies in these areas also show that the faults dip moderately east and record a thrust sense of slip.

4. Methods and closure temperatures of the thermochronology data

The detailed methods of ZrnFT and ZrnHe thermochronology can be found in supplementary data. Considering the reset detrital zircons are relatively young (less than 2 Ma) in the eastern Backbone Range, indicating the high cooling rate (100-200°C/km) (Shen et al., 2020; Liu et al., 2001), we use the CLOSURE program (Brandon et al., 1998) to calculate a bulk effective closure temperature. This calculation allows us to make nominal estimates of the magnitudes and rates of orogenic exhumation. We obtain ca.

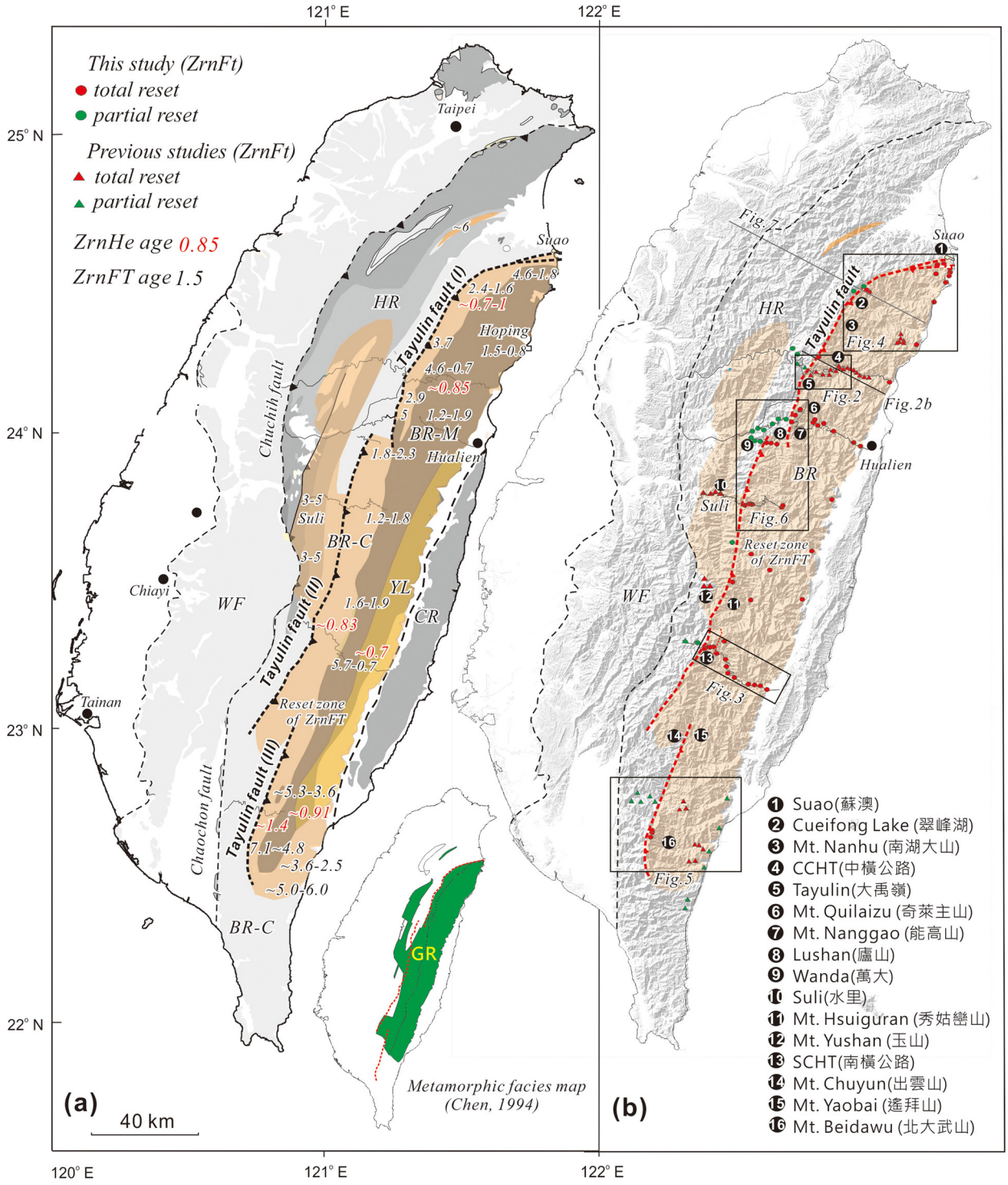

Fig. 1. (a) Simplified geological map of Taiwan (Chen et al., 2000). The light orange color shows the area where ZrnFT ages are reset. The numbers show the reset ZrnFt dates. The inset map shows the area of greenschist facies metamorphic grade (green color) and OOST (red line) (Chen and Wang, 1994). (b) Fault trace of the three segments of the OOST (red dashed line). Numbers show the locations discussed in the text. CP: Coastal Plain; WF: Western Foothills (fold and thrust belt) HR: Hsuehshan Range; BR-C: Backbone Range (Cenozoic slate belt) BR-M: Backbone Ranges (Mesozoic metamorphic complex); YL: Yuli Belt; CR: Coastal Ranges. (For interpretation of the colors in the figure(s), the reader is referred to the web version of this article.)

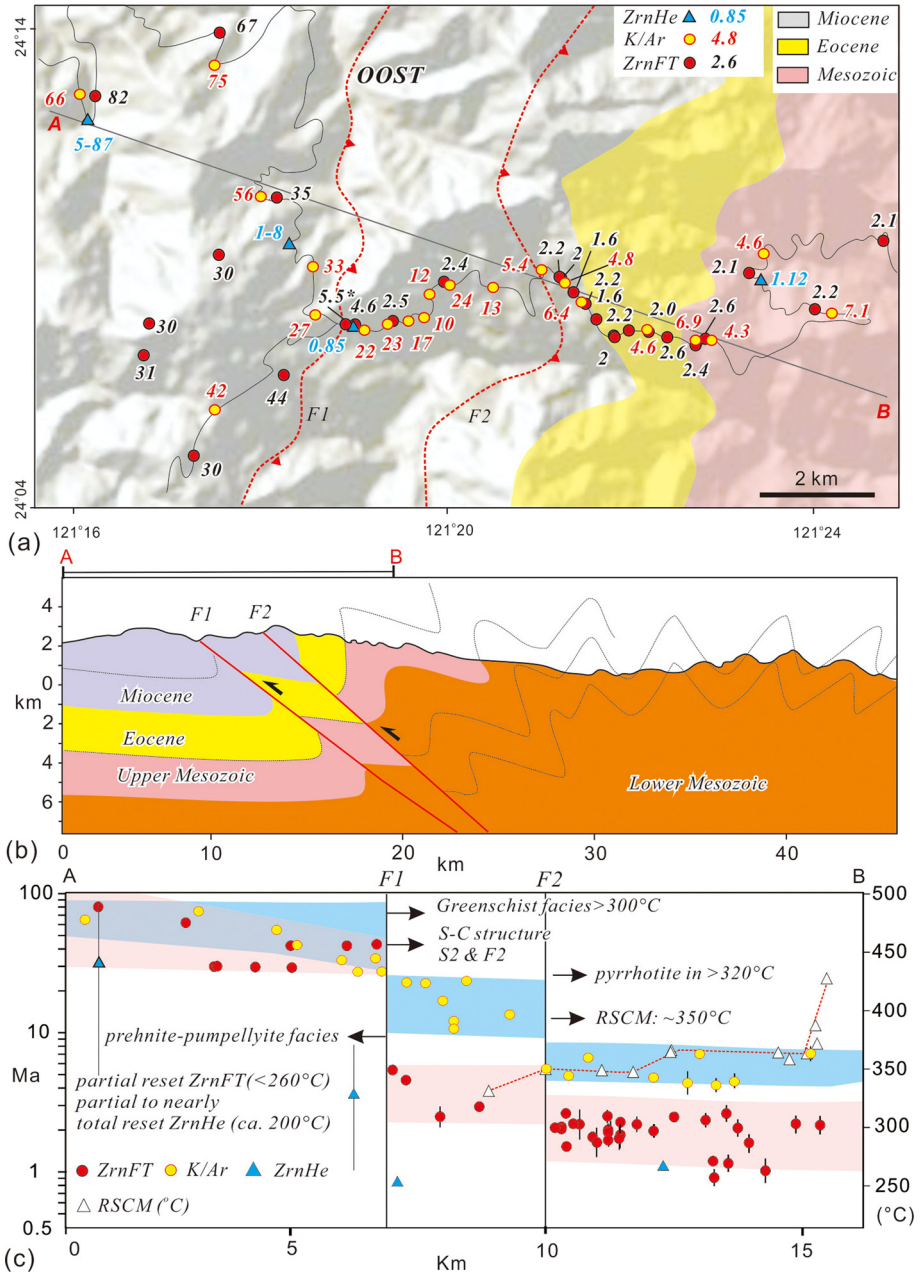

Fig. 2. (a) Geological map and (b) Cross-section of the Taiyulin area along the Central Cross Highway showing trace of OOST and distribution of thermochronologic data used to constrain the map trace of the OOST. Date with a star means youngest reset ZrnFt date. The structural profile is modified from Lo and Yen (1993) and profile location is shown in Fig. 1, which (c) Plot of thermochronology dates versus distance (km) across the OOST. Note that F1 fault offsets the ZrnHe dates, fission track dates, and peak metamorphic temperature. F2 separates the mixing and new growth white mica K/Ar dates. The metamorphic temperature is interpreted to be ca. 350°C in the hanging wall of F2 based on RSCM data. In the footwall of F1, it belongs to the PP zones (200-300°C) and the ZrnFT dates are partial reset, indicating the metamorphic temperature is less than 260°C and it is likely nearly 200°C based on nearly total reset of the ZrnHe (Fig. 2).

260°C (256-263°C) and ca. 210°C (207-214°C) for detrital ZrnFT and ZrnHe, respectively, and a partial retention temperature of ca. 180-260°C for ZrnFT. These temperatures are consistent with the metamorphic conditions in Taiwan. For example, in the upper part of the Lushan Fm., illite crystallinity data indicate paleotemperature in the prehnite-pumpellyite zone (200-300°C), and neither ZrnFT nor ZrnHe dates have been totally annealed. In contrast, where metamorphism is close to or above the greenschist facies zone (ca. 300°C and above), the ZrnFT and ZrnHe dates are totally reset. The ZrnHe system is sensitive to diffusive helium loss between ~200 to <50°C (Reiners et al., 2004; Guenthner et al., 2013), depending primarily on radiation damage in the crystal, cooling rate, mineral chemistry, and grain size. The cooling rate is slow in early stage (Lan et al., 1990; Lee et al., 2006); we therefore consider that the closure temperature for muscovite K/Ar is interpreted to be ~350°C based on Ar diffusion data for muscovite (Harrison et al., 2009) and assuming a 50°C/Ma cooling rate.

5. Results

5.1. Central cross highway transect

Along the Central Cross High Way Transect (CCHT) (Fig. 1 and 2), detailed mapping by Lo and Yen (1993) and Lee and Yang (1994) shows two east-dipping shear zones, F1 and F2, interpreted to be branches of a more regional-scale, east-dipping fault. The hanging wall of the eastern fault, F2, carries Eocene strata that

are overturned to the west (Fig. 2). These overturned strata can be traced from Mt. Nanhu to Mt. Nenggao area (locations shown in Fig. 1). Outcrop-scale S-C shear zones with a top-to-the-west sense of shear and associated crenulation cleavages occur in the hanging wall and footwall of F2. These structures are absent in the Slate Belt east and west of the area around F1 (Lee and Yang, 1994) (Fig. 2b).

The two fault zones along the CCHT separate high and low metamorphic grades (Fig. 2). For example, illite crystallinity, the occurrence of pyrrhotite, and RSCM data indicate greenschist facies metamorphism in the hanging wall of F2 and PP facies in the footwall of F1. Between F1 and F2 metamorphic temperatures are slightly lower, ranging between ca. 300 to 350°C (Beyssac et al., 2007) and K/Ar dates are older (mean 17 Ma) with a wider range (e.g., 10 to 23 Ma) than in the hanging wall of F2. The ZrnFT dates are also slightly older than in the hanging wall and range from 2.4 Ma to 5.5 Ma and the single ZrnHe date of 0.87 Ma. In the footwall of F1 the metamorphic grade is in PP zone and ZrnFT dates are partially to non-reset and range from 31-88 Ma. K-Ar dates range from 42 to 66 Ma and two ZrnHe samples dates yield individual grain dates ranging from 1 to 8 Ma and 5-87 Ma, respectively. All the K/Ar, ZrnFt, and ZrnHe dates are partially to non-reset dates in the footwall of the F1 (Fig. 2) (Tsao et al., 1996; Beyssac et al., 2007). Overall, all of the chronologic systems show a general decrease in age from west to east across the two faults, with some of the systems recording jumps across the faults (e.g., ZrnFT dates across F1 and K/Ar dates across F2) but not in others.

5.2. Southern Cross High Way Transect (SCHT)

Several moderately east-dipping thrust faults have been mapped along the western flank of the Backbone Range along the South Cross-Island Highway Transect (Fig. 1 and 3) (Pelletier and Hu, 1984; Stanley et al., 1981; Tillman and Byrne, 1995). The thrust faults carry older and more metamorphosed rocks in their hanging walls, and stratigraphic units are deformed by west-northwest verging folds with an associated axial planar cleavage. Post-cleavage, outcrop-scale brittle to ductile shear zones, and crenulation cleavages are also locally developed around two of the inferred thrusts, F1 and F2. Although neither of the fault surfaces is exposed, Tillman and Byrne (1995) documented a significant step in cleavage-related penetrative strain with top-to-the west-northwest shear sense and a change in the pattern of cooling ages across F1 (the "Tienshih Fault" in Tillman and Byrne, 1995). F2 and F3 are also marked, in part, by the presence of subsidiary structures, primarily crenulation cleavages, outcrop-scale shear zones, and brittle fault zone also can be observed in the field.

The illite crystallinity, RSCM data, and the occurrence of pyrrhotite in the hanging wall of F1 indicate greenschist facies metamorphism, which contrasts the PP facies in the footwall of F1.

In more detail, K/Ar dates in the hanging wall of F3 range from ∼2 to ∼4 Ma whereas K/Ar dates in the footwall of F1 range from 37-52 Ma. Similarly, ZrnFT dates in the hanging of F3 cluster around 1.5 Ma and ZrnFT dates in the footwall of F1 range from 38 to 70 Ma. RSCM values in the hanging wall of F3 also indicate paleotemperatures increasing eastward from ∼340°C to 450°C, suggesting deeper structure levels are exposed to the east.

Between F3 and F1, K/A dates range from 6.6 to 17.3 Ma and are significantly younger than the 38 to 70 Ma dates obtained from the adjacent footwall of the F1 (Tsao et al., 1996). ZrnFT dates, however, systematically increase from ∼1.5 Ma just above F3 to ∼5.7 Ma just above F2 where there is a sharp step across F2 to ∼20.0 Ma dates (Fig. 3).

Near the F2 fault zone, we obtained two partially reset ZrnFT dates (see asterisks in Fig. 3) that when decomposed, yield two total reset dates of 3.8 Ma and 5.7 Ma (46∼65%).

5.3. Northern Taiwan Transect

Penetrative fabrics in the northern Backbone Range generally strike east-west (Fig. 1). Several thrust faults have also been mapped in the Suao area (Lin and Kao, 1997) (Fig. 4). Detailed structural studies show that faults dip south and display crenulation cleavages and S-C structures in their hanging walls that indicate north-directed shearing (Fig. 4) (Lu et al., 1989). Southwest of the Suao area, Mt. Nanhu areas expose a regional-scale, overturned syncline in the footwall of a major thrust fault (Fig. 1 and 4).

The F1, named as Cueifeng Lake fault (Lin and Lin, 1995), separates prehnite and greenschist grades of metamorphism, as evidenced by the occurrence of the pyrrhotite (Horng et al., 2012) and by the distribution of reset and partially reset ZrnHe and ZrnFT dates. In the hanging wall of F1, reset ZrnFT cooling dates are ca. 4.6-2.2 Ma and the K/Ar ages are ca. 4-6 Ma. Two ZrnHe ages show consistent ages ca 1.0 Ma in the hanging wall of F1 (Fig. 4b), and four ZrnHe ages located on the hanging wall near the Cueufeng Lake yield ages ranging from 0.74 to 0.99 Ma. These results are consistent with reset zircon and apatite fission track ages near Hoping (Fig. 4) that range from 1.5-0.8 Ma and 0.7-0.3 Ma, respectively (Fig. 1 and 4) (Shen et al., 2020).

5.4. Southernmost Taiwan Transect (SMT)

In the southern Backbone Range, two thrust faults have been recognized, the Chaochou fault and Chaokolaitsi fault. The Chaozhou fault crops out along the west flank of the Backbone Range and places deformed slates on unmetamorphosed sediments in the Pingtung Basin or mildly metamorphosed sediments of the fold and thrust belt (Ho, 1986). The Chaokolaitsi fault (Fig. 5b) crops out within the Slate Belt and is marked in the field by northwest verging folds and a crenulation cleavage in its hanging wall (Ho, 1995; Tsao et al., 1996; Lee et al., 2015). K/Ar, ZrnFT, and ZrnHe dates also show a sharp decrease across the inferred position of the fault (Fig. 5), consistent with an east-side-up thrust. K/Ar dates progressively decrease from ∼11-50 Ma to ∼3-7 Ma, ZrnFT dates step from ∼40 Ma to ∼5 Ma, and ZrnHe dates change from partial reset ages to totally reset ages of ∼1.5 Ma across the fault (Fig. 5). This step in ages also coincides with the occurrence of pyrrhotite in the hanging wall east of the fault. The RSCM metamorphic temperature shows differences across the fault (Conand et al., 2020) (Fig. 5).

5.5. Mt. Nenggao Transect

A few km south of the CCHT a transect from Mt. Nenggao (site 7, Fig. 1) to Hualien shows a similar pattern of ZrnFT. Partially reset ZrnFT dates, ranging from 11 Ma to 38 Ma occur in the west and totally reset dates that range from 1.2 to 5 Ma occur in the east. Although detailed structural mapping is limited in this area we infer that the Tailulin fold/fault system separates the eastern and western areas described above.

5.6. Along-strike observations between the Central and Southern Highway Transects

In the Suli transect (Site 10 in Fig. 1 and Fig. 6), a thrust fault has been mapped in the lower Lushan Fm., and all the ZrnFt dates are total reset in the hanging wall and footwall, but the dates are younger (1.4 Ma-1.9 Ma) with higher elevation in the hanging wall and older (3.3 Ma to 3.6 Ma) with lower elevation in the footwall. From Mt. Yusahn to Mt. Hsuiguran (site 11 and 12 in Fig. 1), the ZrnFt reset condition is similar in that the dates are total reset in the hanging wall and footwall, and the dates are younger in the

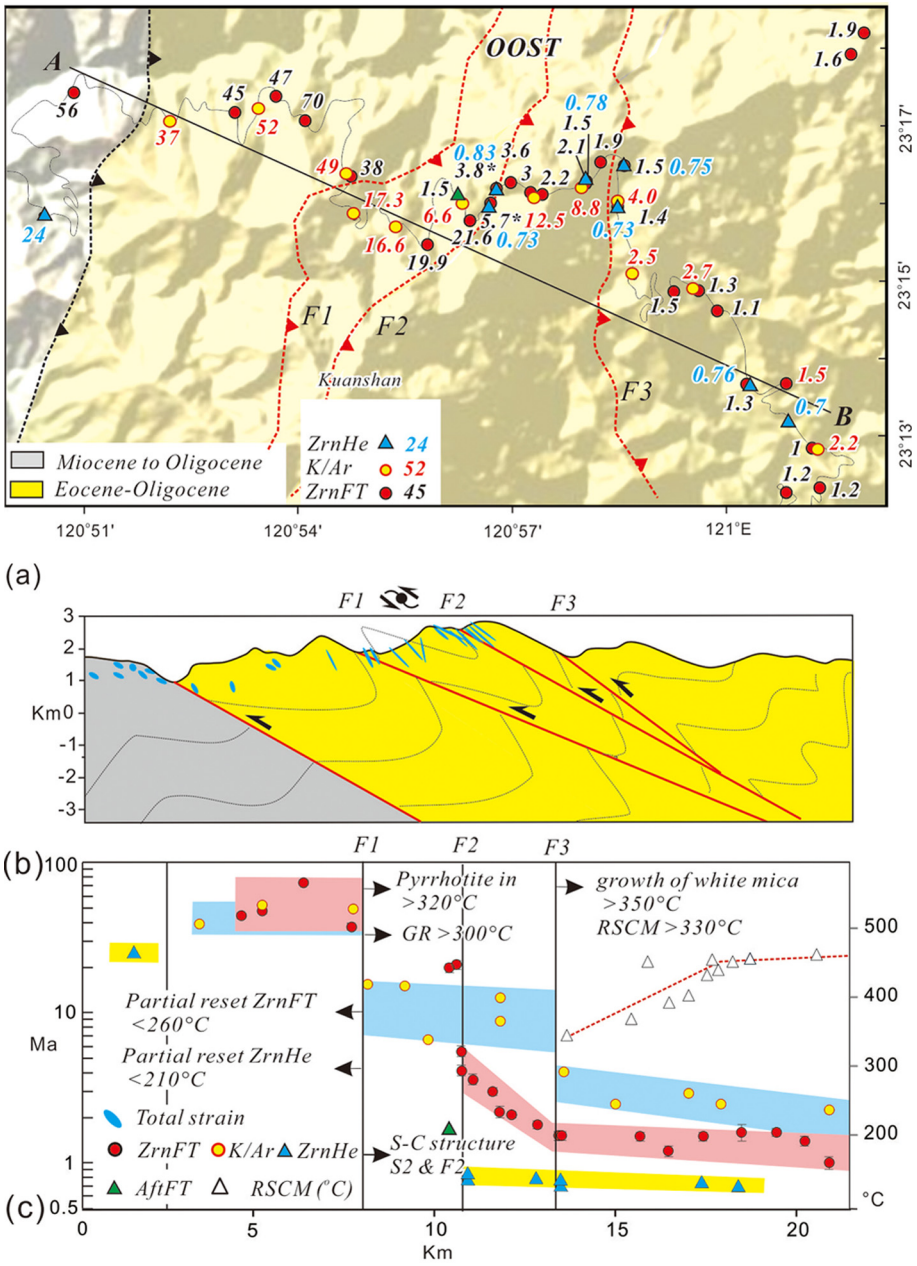

Fig. 3. (a) Geological map and (b) cross-section along the South Cross Highway (modified from Tillman and Byrne, 1995) showing trace of OOST and distribution of thermochronologic ages used to constrain the map trace of the OOST. (c) Plot of thermochronology dates versus distance along the profile. The OOST offsets the ZrnFT, K/Ar, and ZrnHe dates and metamorphic temperature.

hanging wall (1.6 Ma-1.9 Ma) and older in the footwall (3-5 Ma) (Fig. 1 and 6).

Further north, the Wanda area, shows total reset (6.6 Ma to 1.8 Ma) in the hanging wall and partial reset dates (18.4 Ma to 25.7 Ma) in the footwall. We also observe the NW verging F2 with crenulation cleavage development near the fault (Fig. 6).

6. Discussion

6.1. Extending and segmentations of the Tayulin OOST

The Tayulin OOST system has been mapped in many transects, such as the F1 has been named the Cueifeng Lake fault in northern Taiwan, the Tayulin fault in the CCHT transect, the Tienshih Fault in SCHT, and the Chaokolaitsi faults in southern Taiwan (Lin and Kao, 1997; Lo and Yen, 1993; Tillman and Byrne, 1995; Lee et al., 2015). Although the fault has different names, they share similar structural characteristics, such as the west-verging overturn syncline and NW to N-verging ductile shear zones develop on the hanging wall, and fault traces divide different metamorphic phase and different thermochronology dates. All these phenomena indicate that fault is a regional-scale structure.

In northern Taiwan, the Cueifeng Lake fault has been mapped in the Cueifeng Lake area (Lin and Lin, 1995). We connect this fault to an un-named fault in the Suao area (Lin and Kao, 1997), considering the similar attitude of the fault trace, and both faults divide the metamorphic faces. We extend the Cueifeng fault t°CCHT (Tayulin fault system) and then to the Mt. Nenggao area based on the boundary of the GR and PP metamorphic facies, reset and partial reset ZrnFt dates, and overturn syncline develops continuously.

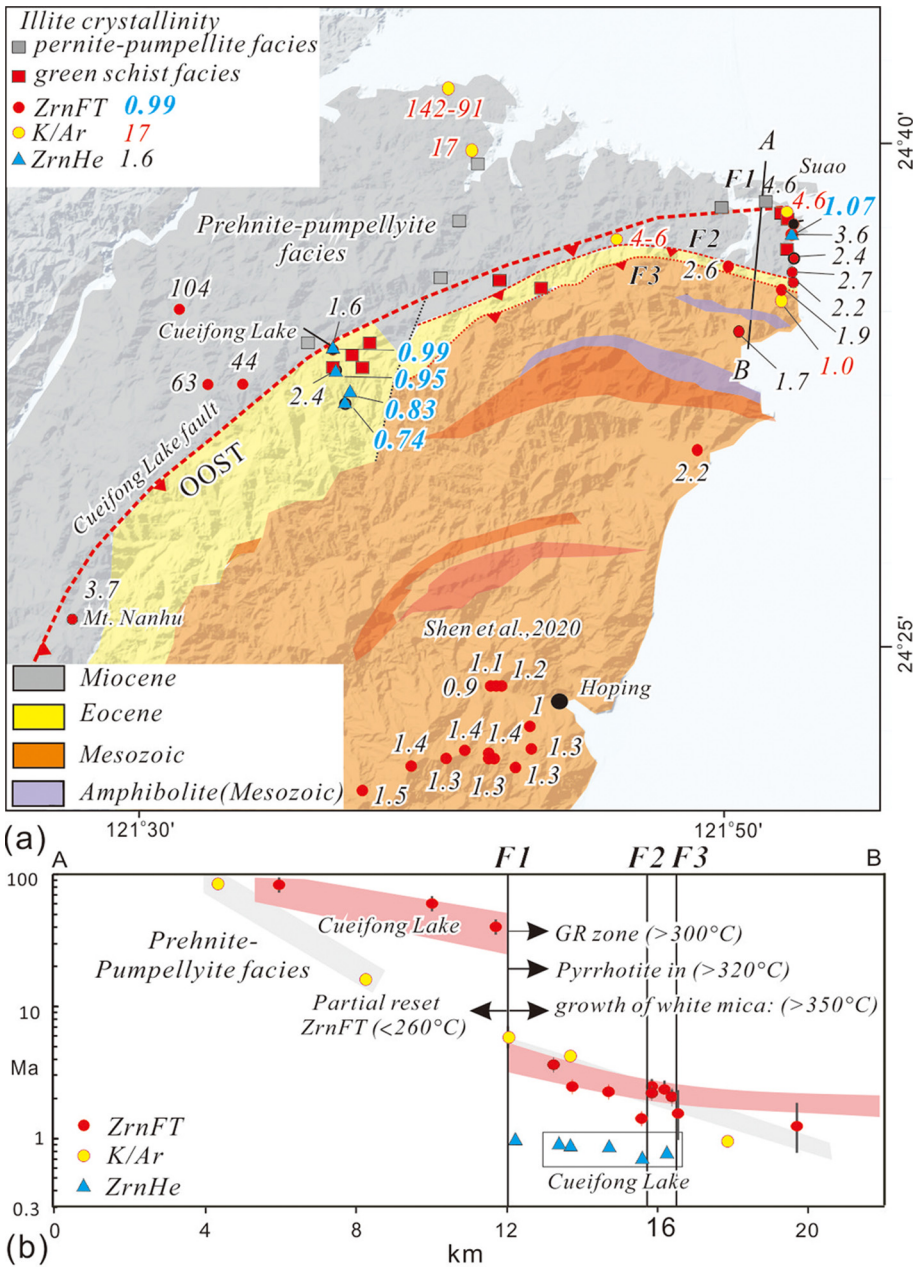

Fig. 4. (a) Schematic geological map showing the trace of OOST and distribution of thermochronologic ages. (B) Plot of thermochronology dates versus distance across the northern Central Range. The OOST offsets the ZrnFT, K/Ar dates, and ZrnHe dates from reset to partial reset and divides the metamorphic facies from GR to PP and occurring the pyrrhotite.

In the Lushan area (site 8 in Fig. 1), the reset ZrnFt boundary steps to the left side, and many NW-trending right-lateral strike-slip faults develop in the Lushan area (Fig. 6).

We suggest a new Tayulin OOST segment develops from south of the Lushan area (Fig. 6). The NW-trending strike-slip faults act as relay structures between two segments. In the Suli area, a thrust fault has been mapped, and we extend this fault trace to the Wanda area; those fault traces are also consistent with metamorphic facies boundary and reset ZrnFt dates on the hanging wall associated with NW-verging shear zones develop near the fault (Fig. 6). We extend segment II from Lushan to SCHT and then Mt. Chuyun (site 14 in Fig. 1) based on fault zone locations, reset and partial reset ZrnFt dates, or younger reset ZrnFt dates (Fig. 1). In the southernmost of Backbone Range, the OOST has been named Chaukolaitsi fault. Considering the fault trace significant changes to the eastern of the segment II, we propose the Chaukolaitsi fault as another segment of the OOST.

Based on structural and geologic mapping, we propose that the Tayulin OOST is a regional-scale structure consisting of three segments (Fig. 1): Segment I extends about 80 to 100 km from Suao to Mt. Nenggao; Segment II extends approximately 120 km from Lushan to Mt. Chuyun (site 14), and Segment III extends about 40 km from Mt. Yaobai to Mt. Baidawu (site 15 and 16 in Fig. 1). The field relation between segments II and III is unknown. A relay zone associated with northwest-striking strike-slip faults develops between segments I and II.

6.2. Structure of the orogenic wedge

Available geologic mapping along the four transects shows a general correlation between the OOST and regional-scale synclines

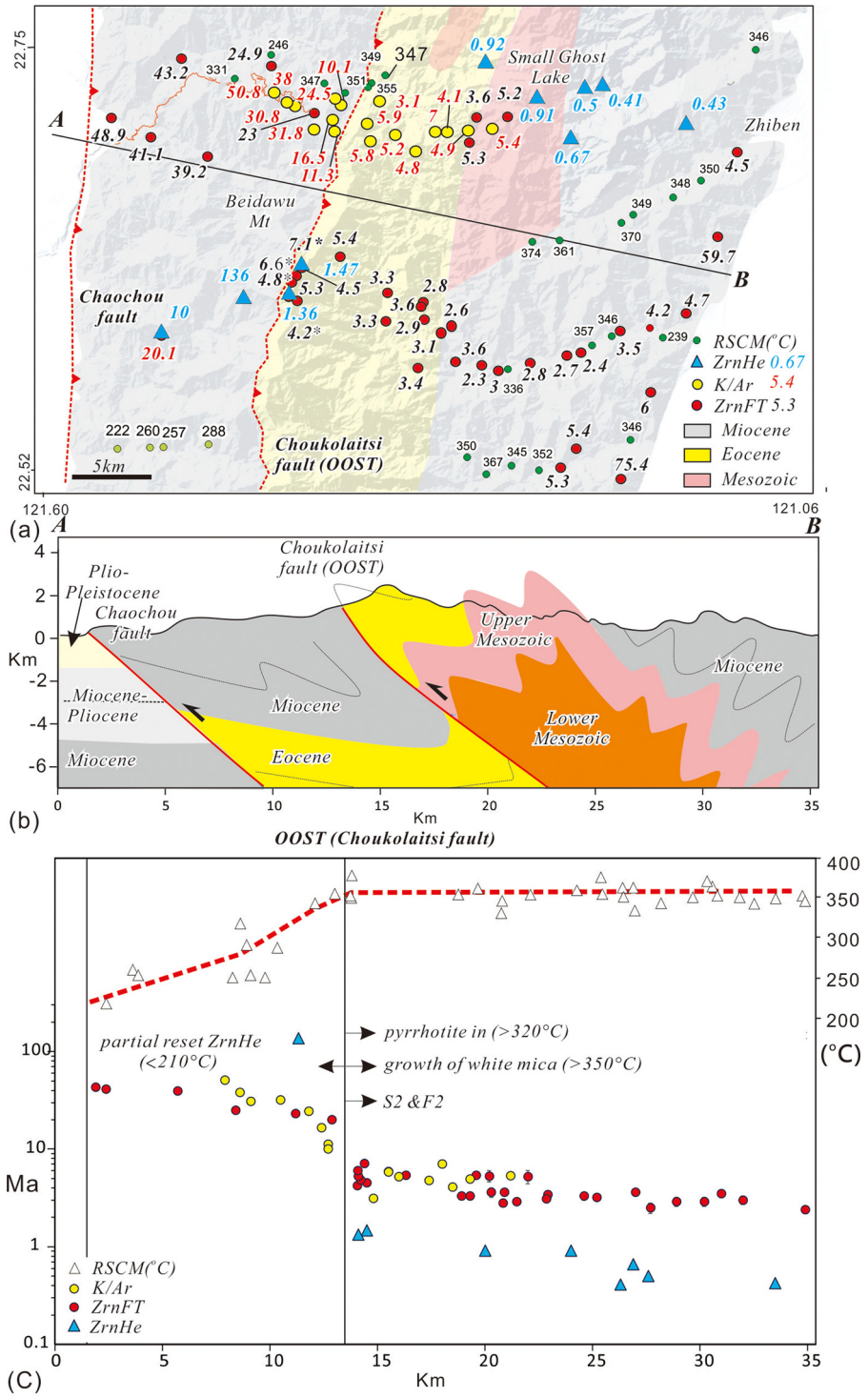

Fig. 5. (a) Schematic geological map showing the trace of OOST and distribution of thermochronologic dates in the southern Central Range. (b) Structural profile across the southern Backbone Range. Two significant faults were mapped in this area. (c) Plot of thermochronology dates versus distance across the southern Central Range. The OOST offsets the ZrnFT, K/Ar dates, and ZrnHe dates from reset to partial reset and divides the metamorphic facies from GR to PP and occurring the pyrrhotite. The ZrnFT dates with stars show decomposed dates.

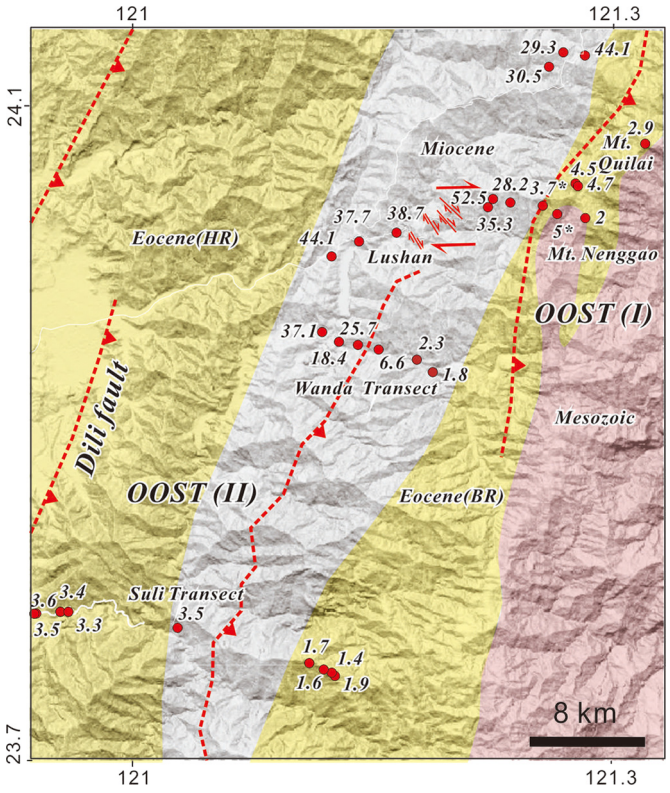

Fig. 6. Schematic geological map between segments I and II of the OOST and distribution of ZrnFt dates (see Fig. 1b). Many strike-slip faults are developed between the offset faults, suggesting a transfer structure.

in the eastern part of the Slate Belt. Along the CCHT, for example, both splays of the OOST crop out near the core of the overturned Tayuling Syncline, which dips east beneath the higher-grade Tailuko Belt. The syncline extends at least 100 km along strike and has an amplitude of several km. The east limb of the syncline dips moderately east, and stratigraphic sequences, including the depositional contact between the Slate and Tailuko Belts, are consistently overturned. Mapping in the Tailuko Belt to the east indicates a series of antiform and synform structures with a higher grade of metamorphism in the belt that indicates deeper erosion (Fig. 2) (Lo and Yen, 1993).

To better understand the deeper structural levels and the role of the OOST, we integrate the structural and thermochronologic results from the CCHT with the distribution of relatively small earthquakes along a profile sub-parallel to the highway (profile B, Carena et al., 2002) and interpretations of the crustal-scale P-wave velocity structure a few km north of the highway (van Avendock et al., 2016). In the P-wave velocity model, the 5 and 5.5 km/sec P-wave velocity contours delineate two relatively large (~8 km amplitude), west-verging antiforms (dashed red line, Fig. 7). The antiforms correlate with the metamorphosed rocks exposed in the Hsüehshan and Backbone Ranges, and the relatively low-velocity unit between the antiforms is consistent with the lower-grade Lushan Formation. The surface trace of the OOST occurs along the boundary between this formation and the higher-grade rocks in the Backbone Range. These observations suggest that the regional-scale overturn syncline mapped along the eastern Slate Belt (Lo and Yen, 1993; Lee and Yang, 1994) correlates with the west-verging synformal structure in the velocity model (Fig. 7). These regional-scale structures also occur above a low-dipping detachment surface illuminated with small earthquakes in this area (Carena et al., 2002). We, therefore, propose that the OOST represents a splay of the main detachment beneath the orogen (Fig. 7).

The projection of the OOST to the depth where the detachment appears to steepen (Fig. 7) also suggests an additional role of the OOST. Because the hanging wall of the OOST carries highly deformed and metamorphosed rocks that are not present elsewhere in the transport direction, the steep section of the detachment fault may represent a ramp utilized by the OOST as it carried higher-grade rocks to higher structural levels. In this scenario, the deformation of the metamorphic core in Taiwan progressed from ductile deformation (i.e., regional-scale antiforms and synforms; Fig. 2 and 5) to brittle faulting along a major west-verging thrust system that offsets metamorphic facies.

6.3. Offset and slip history of the Tayulin OOST

The slip and slip history along the different segments of the OOST can be estimated from the offset in metamorphic grade, fission-track dates of the totally detrital zircon grains, K/Ar dates, and from apparent age-elevation profiles in the hanging wall.

In CCHT, the K/Ar dates are total reset, ranging from ~5-7 Ma in the hanging wall of the F3 (Tsao et al., 1996). The closure temperature of K/Ar is ca. 350°C, and the RSCM maximum metamorphic temperature is also 350°C. Considering that the maximum metamorphic temperature is the same as the closure temperature of the K/Ar, the 5-7 Ma dates indicate the timing of metamorphism or the initial stage of the exhumation. This interpretation is supported by the occurrence of new, relatively large mica grains along cleavage planes in rocks.

Between F1 and F2, the 10-24 Ma K/Ar dates are interpreted as a mixture of source and in-situ metamorphic ages, whereas the 5.5-2.4 Ma ZrnFT and 0.85 Ma ZrnHe dates are interpreted as cooling ages.

In the footwall of the F1, both ZrnFt and ZrnHe dates are partial reset inferring the metamorphic temperature is less than the closure temperature of ZrnHe, 210°C; by contrast, the metamorphic temperature is higher than 350°C, inferring the 140°C of vertical throw occurred after this time (Fig. 2).

Fully reset ZrnFT dates in the hanging wall are younger than the K/Ar dates of mica, consistent with the lower annealing temperatures for fission tracks in zircon and yield dates of ~2 Ma. These young ages suggest that the slip and associated cooling is continuous after about 2 Ma. Finally, two fully reset ZrnHe dates along this transect are younger than nearby ZrnFT ages, consistent with the lower temperature dependence for He diffusion in zircon, and yield ages between 0.7 and 1.47 Ma. Although only two dates are available, the older date occurs in the hanging wall of F3, which is inconsistent with the offset in the K/Ar and ZrnFT dates. The younger date occurs just above F1, suggesting slip is continuous along F1 at ~0.7 Ma.

Along the SCHT, the F1, associated with post-cleavage, brittle to ductile shear zones, which has been interpreted to be relatively young and probably out-of-sequence relative to deformation in the foreland (Tillman and Byrne, 1995). Similar deformation patterns have been observed in F2 and F3. The fault system along the SCHT (F1, F2, and F3) appears to record significant displacement as individual faults correlate with abrupt steps in the paleotemperature and cooling age patterns (Fig. 3).

From F3 to F1, the K/Ar dates range from total reset to partial reset dates, consistent with west-side-up displacement (Tsao et al., 1996). ZrnFT dates systematically increase from ~1.5 Ma just above F3 to ~5.7 Ma just above F2, where there is a sharp step across F2 to ~20.0 Ma dates (Fig. 3).

Near the F2 fault zone, the oldest reset dates represent the time of thrusting of F2 from ~3.8-5.7 Ma. The gradient in ZrnFT between F3 and F2 and the sharp step across F2 may represent the frontal limb of the anticline above thrust with the U-shaped pattern (Lock and Willett, 2008). The ZrnHe dates are similar at

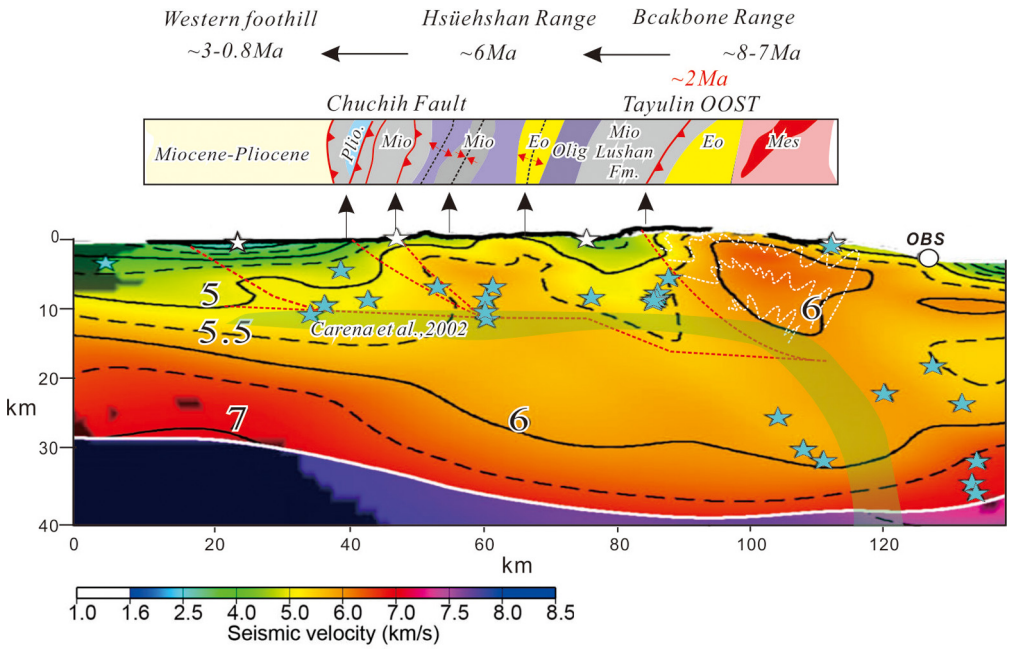

Fig. 7. Comparing the surface geology data with the P-wave tomography images by Van Avendonk et al. (2016) are annotated with our interpretation of the regional-scale structures (location is shown in Fig. 1b). The green shadow area is the possible detachment based on small earthquake distribution (Carnea et al., 2002). The Explosive shots (white stars), ocean-bottom seismometer (white circles). Seismic velocities are contoured at 1.0 km s–1 (solid) and 0.5 km s–1 (dashed) intervals. White solid line marks the boundary of the Moho of Eurasian crust. Light blue stars mark the projected location of local earthquakes used in the tomography inversion.

0.7-0.8 Ma across the F2 and F3 may indicate the reflect F3 is not active during that time. Considering the youngest ZrnHe dates is ~0.7 Ma in the hanging wall of the F2 indicates thrusting along F1 and F2 continued to at least ~0.7 Ma. Overall, the K/Ar, ZrnFT and ZrnHe dates in the hanging wall of F3 are consistent with continuous cooling, assuming generally attributed closure temperatures.

In SMT, it includes the Small Ghost Lake transect and Beidawu transect. The oldest reset K/Ar dates are ~5-7 Ma along the Small Ghost transect, similar t°C CHT and representing the timing of metamorphism or early-stage exhumation (Fig. 5). On the hanging wall of the fault, the ZrnHe dates are less than 1.5 Ma, indicating the fault continues to be active at this time. The total reset of K/Ar dates indicates the metamorphism is higher than 350°C on the hanging wall, and the ZrnHe dates are partial reset inferring the metamorphic temperature is less than 210°C in the footwall. The fault, therefore, offsets the 140°C metamorphic temperature. The RSCM data also show that the metamorphic temperatures are offset across the fault (Fig. 5c). The RSCM metamorphic temperatures have been interpreted to be inherited from the Paleogene rift evolution in the southern Backbone Range (Conand et al., 2020). Both ZrnHe and ZrnFt dates are partial reset in the footwall, indicating that metamorphic temperature is lower than 210°C; the RSCM temperatures, by contrast, are high than 250°C in the nearby area that supports the interpretation of inherited metamorphic temperature for RSCM in the footwall. Along the Small Lake transect, the RSCM temperatures are nearly 350°C, and the K/Ar dates have been reset with large mica growth, indicating the metamorphic temperature could be related to the orogenic process. The RSCM metamorphic temperature records the maximum metamorphic temperature (Beyssac et al., 2007), and it represents the inherited metamorphic temperature or the metamorphism during the orogenic process, depending on which mechanisms have a higher metamorphic temperature. Although the mechanism of the metamorphic temperature is still vague, the RSCM temperature shows about 100°C offset across the fault, which is consistent with thermochronology data.

Apparent age-elevation profiles from the hanging wall can also yield valuable information about the slip history, assuming slip on the OOST leads to crustal thickening and an increase in topographic relief, which then drives higher rates of erosion-driven exhumation. We also assume a constant geothermal gradient over the duration of faulting. To construct age-elevation profiles from each transects, we combine new and previously published data from the hanging walls of the OOST along each transects (Fig. 8).

In the northern Taiwan transect, ZrnFT, Aft, ZrnHe, and ZrnFT data show a significantly higher rate of 3.4 mm/yr to 4.3 mm/yr from 1.5 Ma to 0.3 Ma and a slow rate from 3.7 Ma to 1.5 Ma. In the CCHT and Mt. Nenggao transect, which lies about 20 km to the south, the integrated data set shows exhumation rates of ca. 2.6-2.9 mm/yr from 2 Ma to 0.5 Ma with significantly slow exhumation rates before 2 Ma (Fig. 8b). These rates are consistent with previous results (Hsu et al., 2016) (Fig. 8b). In the SCHT area, the exhumation rate is accelerating from 2.3 mm/yr to 6.5 mm/yr from ca. 1.9 Ma to 0.5 Ma and a significantly slower rate from ca. 5.7 Ma-2 Ma (Fig. 8c). In the area of the SMT, an integrated set of two new ZrnHe ages near the summit of Mt. Beidawu with six ZrnHe ages from near Small Ghost Lake to Zhiben (Hsu et al., 2016) shows a constant exhumation rate of 2.3 mm/yr from ca. 1.5 Ma to 0.3 Ma. In contrast, ZrnFT ages from the watersheds east of Mt Beidawu show a slow exhumation rate ca. 0.7 mm/yr from ca. 7 Ma to ca. 2.2 Ma (Lee et al., 2015; Mesalles et al., 2014 and new data) (Fig. 8d).

In the SMT, the ZrnFt date records the slow exhumation rate from 7-2 Ma. In NT transect, few ZrnFt dates also show slow exhumation before 2 Ma. The multiple thermochronology system shows a slower cooling rate from ca. 8 Ma to 2 Ma in the Hoping area (Lan et al., 1990; Lee et al., 2006), which is consistent with the slow exhumation process in the early-stage exhumation. Mesalles et al. (2014) have interpreted that the older ZrnFt reset dates result from cooling from below by the lower underthrusting plate characteristic of subduction. The 7 Ma age also shows in K/Ar date, which is related to metamorphism or early stage exhumation, and considering the linear age-elevation relationship from ca. 7-2 Ma with a slow exhumation rate in southernmost Taiwan orogeny, we prefer that the older reset ZrnFt dates are related to the uplift and cooling process during the wedge deformation.

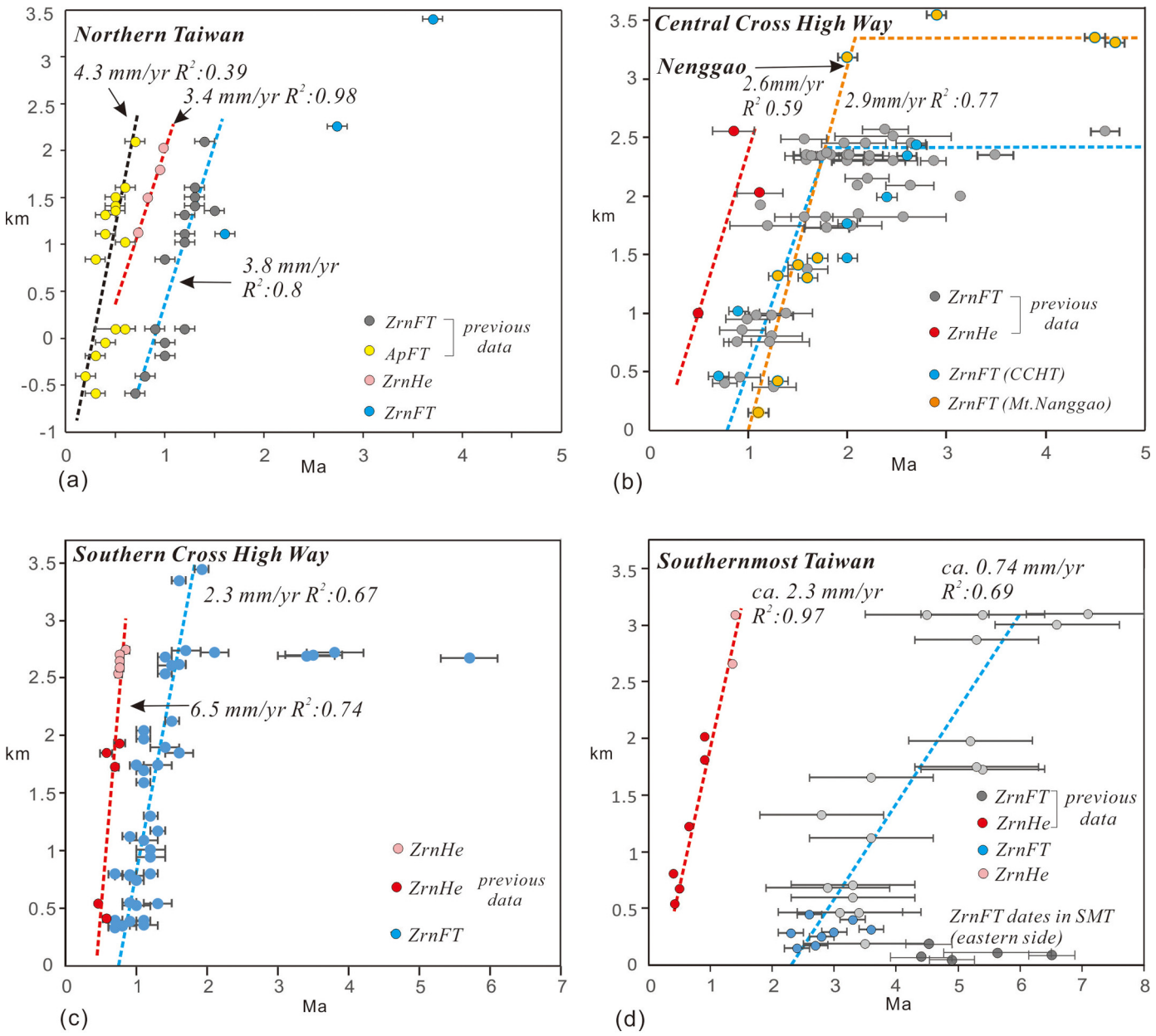

Fig. 8. Vertical apparent age-elevation profiles from the hanging wall of the OOST. (a) Northern Taiwan transect, including Hoping area (data from Shen et al., 2020), Negative elevation means the samples collected from drilling; (b) Central Cross Highway transect and Mt. Nenggao transect; (c) Southern Cross Highway transect; (d) Southernmost Taiwan transect. Profiles show exhumation rates ranging from ~2.3 to ~6.5 mm/yr except for samples older than about 2 Ma. Sample older than about 2 Ma in southernmost Taiwan also shows a substantially slower rate of exhumation, ~0.7 mm/yr. Overall, from ca. 2 Ma to 0.3 Ma, the exhumation rate accelerates to ca. 2.3-6.5 mm/yr.

Overall the apparent age-elevation of ZrnFt dates shows a higher exhumation rate after 2 Ma. The accelerating exhumation at ca. 2 Ma is also recorded by the first arrival of reset ZrnFT grains with 2 Ma ages in the Luzon forearc basin (Kirstein et al., 2009), an increasing rate of sedimentation at 2 Ma (Dorsey and Lundberg, 1988).

The oldest reset dates of the K/Ar and ZrnFt are 5-7 M, indicating the timing of the early stage of faulting activity. However, we consider the slip amount relatively small because of the slow exhumation rate from 7-2 Ma.

If we assume that the acceleration in exhumation cooling at ~2 Ma signals the initial activity of the OOST and that the fault dips ~45°, then ~4.7-2.8 km of vertical separation (using a thermal gradient of 30-50°C/km and the observed offset of 140°C), suggests ~6.6-4 km of displacement along the OOST. If the fault initiation at 2 Ma with 2.5 km/my indicates 5 km vertical displacement, that is consistent with the estimate from offsetting the metamorphic temperature.

Alternatively, if we assume that measured cooling rates and inferred exhumation in the hanging wall, which range from ~2.3 km/my to 6.5 km/my, are equivalent to rock uplift rates, then 140°C of vertical offset (~4.7-2.8 km) would take ~2-1.2 my using the slower rate and ~0.7-0.4 my using the higher rate. The slip rate along a 45° dipping OOST would be significantly higher, ranging from 43.2 km/my to >9 km/my. Both estimates are substantially higher than most active faults in Taiwan.

6.4. Growth and thickening of the orogenic wedge

Various thickening mechanisms have been proposed to accommodate frontal accretion, ranging from distributed ductile deformation (e.g., penetrative cleavages) to a combination of brittle

or ductile underplating beneath the wedge to more focused slip on major, orogen-scale thrust faults, often referred to as out-of-sequence structures (Morley, 1988). Because thickening is required to occur in the rear or hinterland portion of the orogen, the various mechanisms may also facilitate the exhumation of high-grade metamorphic rocks. These exposed sequences present their own challenges, however, because they are often multiply deformed and metamorphosed, and stratigraphic and tectonostratigraphic sequences are difficult to recognize and correlate along or across strike. The structural history of the higher-grade rocks in Taiwan is debated in part for this reason (Barr and Dahlen, 1989; Fuller et al., 2006; Simoes et al., 2007; Malavieille, 2010; Tillman and Byrne, 1995; Conand et al., 2020). However, the relatively small size of the Taiwan orogen and the well-developed scientific infrastructure allowed us to circumvent this challenge by utilizing high-resolution datasets that are not always available in other areas.

For example, the high concentration of earthquakes increased the resolution of both the décollement (Carena et al., 2002) and the velocity model; an offshore array of OBS instruments also increased the resolution of the velocity model (van Avendock et al., 2016). Our study highlights the importance of combining thermochronology dates, structural data, and seismic tomography to identify the structural characteristic of the hinterland and provide an example for other studies of orogens.

The integrated data sets across the OOST and the metamorphic core and its sedimentary cover in Taiwan argue for a combination of thickening mechanisms. Our preferred interpretation is that thickening early in the collision appears to have been accommodated by regional-scale folding that involved both the Tailuko and Slate Belts at mid-crustal levels above the detachment fault (e.g., near peak metamorphic conditions ~450-500°C and 15-18 km). Involvement of the Tailuko Belt, which is only exposed east of the syncline and the associated OOST, suggests the fold formed in the hanging wall of a major ramp in the decollement (Fig. 7). The geochronology data across the overturned limb of the fold also suggest that folding started after peak metamorphism at ~7 Ma; an interpretation that is consistent with the oldest reset biotite Ar-Ar date of 8 Ma from the metamorphic core (Lo and Onstott, 1995). In Hsuehshan Range, the oldest cooling ages are ca. 6 Ma based on A-Ar and ZrnFT ages (Chen et al., 2018; Lee et al., 2015). In the fold and thrust belt, Mouthereau et al. (2001) studied the faulting history of southwestern Taiwan, which shows the faulting start from 5 Ma in the east and migrates to the west at 3-1.6 Ma and 0.8 Ma in the westernmost. These ages are therefore consistent with the notion of in-sequence deformation in growth of the orogen (Fig. 7).

The underplating model has been proposed to be the primary mechanism of exhumation Backbone Range. However we do not observe apparent normal shear zones near the OOST (see for example Fig 3 in Malavieille, 2010) but a significant thrust. We, therefore, propose that after ~2 Ma, slip on a crustal-scale OOST resulted in relatively rapid uplift and exhumation, and may have been the primary mechanism for the exhumation of the Backbone Range of the Taiwan orogen.

7. Conclusions

Based on thermochronology, structural data, paleotemperature data, and seismic tomography, we identify a significant OOST in the metamorphic core of the orogen that appears to have been active from about 2 Ma to as recently as 0.3 Ma. The OOST can be separated into three segments with ca. 270 km total length and apparent age-elevation profiles suggest a relatively slow exhumation rate in the early stages from ca. 8 Ma to 2 Ma, which could be related to regional-scale folding and foliation development. A subsequent increase in exhumation rate between 2.3-6.5 mm/yr after 2 Ma resulted from slip on a crustal-scale OOST that is the primary mechanism for the exhumation of the Backbone Range.

CRediT authorship contribution statement

Yuan-Hsi Lee: Supervision, conceptualization ideas, writing and editing original draft, Visualization

Timothy B. Byrne: writing and editing original draft and visualization

Wei Lo: resources including collect the samples and field works

Shao-Jyun Wang: data curation, analyze the ZrnFT dates

Shuh-Jong Tsao: data curation, analyze the ZrnFT dates

Cheng-Hong Chen: data curation, analyze the ZFT dates

Han-Cheng Yu: analysis the ZrnHe dates

Xin-Bin Tan: data curation, separate the experimental minerals

Matthijs van Soest: data curation, analyze the ZrnHe dates

Kip Hodges: analyze the ZrnHe and K/Ar dates and editing the original draft

Mesalles Lucas: data curation and editing original draft

Holden Robinsion: data curation, analyze the ZrnHe dates

Julie C. Fosdick: data curation, analyze the ZrnHe dates

Declaration of competing interest

The authors declare that they have no known competing financial interests or personal relationships that could have appeared to influence the work reported in this paper.

Acknowledgements

This study was funded by the Ministry of Science and Technology, Taiwan, R.O.C., the Fundamental Research Funds for the Institute of Geology, China Earthquake Administration (IGCEA2004), the US National Sciences Foundation (EAR-1220453 to Byrne), and the Geological Society of America Graduate Student Research Grant Program. The Basin Analysis and Helium Thermochronology Laboratory is supported by National Science Foundation Award EAR 1735492. One of the authors, Shuh-Jong Tsao, passed away during the review period and this article commemorates his many contributions to understanding orogenic processes in Taiwan. Dr. Tsao was an early leader in K-Ar dating, illite crystallinity, and fission track dating in Taiwan and these early works continue to be referenced and incorporated into new ideas and models of the orogen, including the research presented here.

Early versions of the manuscript were improved significantly by thoughtful reviews by two anonymous reviewers and the editor, Alex Webb.

Funding

All of the sources of funding for the work described in this publication are acknowledged below:

Ministry of Science and Technology, Taiwan, R.O.C., (MOST-107-2116-M-194-002-MY3)
National Science Council, Taiwan R.O.C., (NSC80-0202-M-002-23).
Fundamental Research Funds for the Institute of Geology, China Earthquake Administration (IGCEA2004).
US National Sciences Foundation (EAR-1220453 and EAR 1735492)
Geological Society of America (GSA-13177-21).

Appendix A. Supplementary material

Supplementary material related to this article can be found online at https://doi.org/10.1016/j.epsl.2022.117711.

References

Barr, T.D., Dahlen, F.A., 1989. Brittle frictional mountain building: 2. Thermal structure and heat budget. J. Geophys. Res. 94, 3923–3947.

Beyssac, O., Simoes, M., Avouac, J.P., Farley, K.A., Chen, Y.G., Chan, Y.C., Goffé, B., 2007. Late Cenozoic metamorphic evolution and exhumation of Taiwan. Tectonics 26, TC6001. https://doi.org/10.1029/2006TC002064.

Brandon, M.T., Roden-Tice, M.K., Garver, J.I., 1998. Late Cenozoic exhumation of the Cascadia accretionary wedge in the Olympic Mountains, Northwest Washington State. Geol. Soc. Am. Bull. 110 (8), 985–1009.

Conand, C., Mouthereau, F., Ganne, J., Lin, A.T.S., Lahfid, A., Daudet, M., et al., 2020. Strain partitioning and exhumation in oblique Taiwan collision: role of rift architecture and plate kinematics. Tectonics 38. https://doi.org/10.1029/2019TC005798.

Carena, S., Suppe, J., Kao, H., 2002. Active detachment of Taiwan illuminated by small earthquakes and its control of first-order topography. Geology 30 (10), 935–938.

Chapple, W.M., 1978. Mechanics of thin-skinned fold-and-thrust belts. Geol. Soc. Am. Bull. 89, 1189–1198.

Chen, C. H., et al., 2000. 1:500000 Geologic map of Taiwan. Central Geological Survey, MOEA, Taiwan, R.O.C.

Chen, C.T., Chan, Y.C., Lo, C.H., Malavieille, J., Lu, C., Tang, J.T., Lee, Y.H., 2018. Basal accretion, a major mechanism for mountain building in Taiwan revealed in rock thermal history. J. Asian Earth Sci. 152, 80–90.

Chen, C.-H., Wang, C.-H., 1994. Explanatory notes for the metamorphic facies map of Taiwan. Centr. Geol. Surv. Spec. Publ., vol. 2. MOEA, Taiwan, R.O.C., 2nd ed., 51 pp.

Chen, W.S., Chung, S.L., Chou, Z.Z., Shao, W.Y., Lee, Y.H., 2017. A reinterpretation of the metamorphic Yuli belt. In: Evidence for a Middle-Late Miocene Accretionary Prism in Eastern Taiwan Tectonics, Vol. 36(2), pp. 188–206.

Clark, M.B., Fisher, D.M., Lu, C.-Y., Chen, C.-S., 1993. The Hsüehshan Range of Taiwan: a crustal-scale pop-up structure. Tectonics 12 (1), 205–217.

Davis, D., Suppe, J., Dahlen, F.A., 1983. Mechanics of fold-and-thrust belts and accretionary wedges. J. Geophys. Res. 88, 1153–1172.

Dorsey, R., Lundberg, N., 1988. Lithofacies analysis and basin reconstruction of the Plio—Pleistocene collisional basin, coastal range of eastern Taiwan. Acta Geol. Tawain. 26, 57–132.

Fuller, C.W., Willett, S.D., Fisher, D.M., Lu, C.Y., 2006. A thermomechanical wedge model of Taiwan constrained by fission-track thermochronometry. Tectonophysics 425, 1–24.

Harrison, T.M., Celerier, J., Aikman, A.B., Hermann, J., Heizler, M.T., 2009. Diffusion of 40Ar in muscovite. Geochim. Cosmochim. Acta 73, 1039–1051.

Ho, C.S., 1986. A synthesis of the geologic evolution of Taiwan. Tectonophysics 125, 1–16.

Ho, H.C., 1995. Study of stratigraphy and geologic structure along the route from Santi t°Chinpenchushan, South Taiwan. Master thesis. National Taiwan University.

Guenthner, W.R., Reiners, P.W., Ketcham, R.A., Nasdala, L., Giester, G., 2013. Helium diffusion in natural zircon: radiation damage, anisotropy, and the interpretation of zircon (U–Th)/He thermochronology. Am. J. Sci. 313 (3), 14–198. https://doi.org/10.2475/03.

Horng, C.S., Huh, C.A., Chen, K.H., Lin, C.H., Shea, K.S., Hsiung, K.H., 2012. Pyrrhotite as a tracer for denudation of the Taiwan orogen. Geochem. Geophys. Geosyst. 13, Q08Z47. https://doi.org/10.1029/2012GC004195.

Hsu, W.H., Byrne, Timothy B., William Ouimet, W., Lee, Y.H., Chen, Y.G., van Soest, M., Hodges, K., 2016. Pleistocene onset of rapid, punctuated exhumation in the eastern Central Range of the Taiwan orogenic belt. Geology 22. https://doi.org/10.1130/G37914.1.

Keyser, W., Tsai, C.H., Iizuka, Y., Oberhänsli, R., Ernst, W.G., 2015. High-pressure metamorphism in the Chinshuichi area, Yuli belt, eastern Taiwan. Tectonophysics 692, 191–202.

Kirstein, L.A., Fellin, M.G., Willett, S.D., Carter, A., Chen, Y.G., Garver, J.I., Lee, D.C., 2009. Pliocene onset of rapid exhumation in Taiwan during arc-continent collision: new insights from detrital thermochronometry. Basin Res. 22, 270–285.

Konstantinovskaia, E., Malavieille, J., 2005. Erosion and exhumation in accretionary orogens: experimental and geological approaches. Geochem. Geophys. Geosyst. 6, Q02006. https://doi.org/10.1029/2004GC000794.

Lan, C.Y., Lee, T., Wang, C.L., 1990. The Rb–Sr isotopic record in Taiwan gneisses and its tectonic implication. Tectonophysics 183, 129–143.

Lee, Y.H., Yang, C.N., 1994. Structural Evolution in the Tayulin Area of the Central Range Bulletin, Central Geological Survey (Taiwan), Vol. 9, pp. 77–105.

Lee, Y.H., Byrne, T., Wang, W.H., Wei, L., Rau, R.J., Lu, H.Y., 2015. Simultaneous mountain building in the Taiwan orogenic belt. Geology. https://doi.org/10.1130/G36373.1.

Lee, Y.H., Chen, C.C., Liu, T.K., Ho, H.C., Lu, H.Y., Lo, W., 2006. Mountain building mechanism in southern central range of Taiwan Orogeny Belt - from accretionary wedge deformation to arc-continental collision. Earth Planet. Sci. Lett. 252, 413–422.

Lin, C.W., Kao, M.C., 1997. 1:50000 scale Suao geological map, Central Geological Survey, MOEA.

Lin, C. W., Lin, W.H., 1995. 1:50000 scale Sanshingeological map, Central Geological Survey, MOEA.

Liu, T.K., Hsieh, S., Chen, Y.G., Chen, W.S., 2001. Thermo-kinematic evolution of the Taiwan oblique-collision mountain belt as revealed by zircon fission-track dating. Earth Planet. Sci. Lett. 186, 45–56.

Lock, J., Willett, S., 2008. Low-temperature thermochronometric ages in fold-and-thrust belts. Tectonophysics 456, 14–162.

Lo, C.H., Onstott, T.C., 1995. Rejuvenation of K–Ar systems for minerals in the Taiwan Mountain belt. Earth Planet. Sci. Lett. 131, 71–98.

Lo, W., Yen, T.P., 1993. 1:50000 scale geological map of the Tayulin, Central Geological Survey, MOEA.

Lu, C.Y., Sun, L.J., Lee, J.C., Liou, Y.S., Liou, T.S., 1989. The shear structures in the Miocene Lushan formation of the Suao area, eastern Taiwan. Proc. Geol. 32 (2), 121–137.

Malavieille, J., 2010. Impact of erosion, sedimentation, and structural heritage on the structure and kinematics of orogenic wedges: analog models and case studies. GSA Today 20 (1). https://doi.org/10.1130/GSATG48A.1.

McQuarrie, N., Tobgay, T., Long, S.P., Reiners, P.W., Cosca, M.A., 2014. Variable exhumation rates and variable displacement rates: documenting recent slowing of Himalayan shortening in western Bhutan. Earth Planet. Sci. Lett. 386, 161–174.

Mesalles, L., Mouthereau, F., Bernet, M., Chang, C.P., Lin, A.T.S., Fillon, C., Sengelen, X., 2014. From submarine continental accretion to arc-continent orogenic evolution: the thermal record in southern Taiwan. Geology 42, 907–910. https://doi.org/10.1130/G35854.1.

Moore, G., Banks, N., Taira, A., Kuramoto, S., Pangborn, E., Tobin, H., 2007. Three-dimensional spaly fault geometry and implications for tsunami generation. Science 318 (5853), 1128–1131.

Morley, C.K., 1988. Out-of-sequence thrusts. Tectonics 7 (3), 539–561.

Mouthereau, F., Lacombe, O., Deffontaines, B., Angelier, J., Brusset, S., 2001. Deformation history of the southwestern Taiwan foreland thrust belt: insights from tectono-sedimentary analyses and balanced cross-sections. Tectonophysics 333, 293–322.

Pelletier, B., Hu, H.N., 1984. New structural data along two transects across the southern half of the central range of Taiwan. Mem. Geol. Geol. Soc. China 6, 1–19.

Reiners, P.W., Spell, T., Nicolescu, S., Zanetti, K., 2004. Zircon (U–Th)/He thermochronometry: He diffusion and comparisons with 40Ar/39Ar dating. Geochim. Cosmochim. Acta 68, 1857–1887.

Shen, T.T., Liu, T.K., Huang, S.Y., Hsieh, P.S., Wu, C.Y., 2020. Post-collisional exhumation and geotherm pattern in northern Tanana°complex, northeastern Taiwan. Terr. Atmos. Ocean. Sci. 31, 369–381. https://doi.org/10.3319/TAO.2019.04.06.01.

Simoes, M., Avouac, J.P., Beyssac, O., Goffe, B., Farley, K.A., Chen, Y.G., 2007. Mountain building in Taiwan: a thermokinematic model. J. Geophys. Res. https://doi.org/10.1029/2006JB004824.

Stanley, R.S., Hill, L.B., Chang, H.C., Hu, H.N., 1981. A transect through the metamorphic core of the central mountains, southern Taiwan.pdf. Mem. Geol. Soc. China 4, 443–473.

Suppe, J., 1981. Mechanics of mountain building and metamorphism in Taiwan. Mem. Geol. Soc. China 4, 67–89.

Tillman, K.S., Byrne, T., 1995. Kinematic analysis of the Taiwan Slate Belt. Tectonics 14 (2), 322–341.

Tsao, S., Law, E., Ho, H.C., Lee, Y.H., Jiang, W.T., Chen, C.H., 1996. The geological significances of K/Ar ages of metapelites from the Central Range, Taiwan. Bull. Central Geol. Surv. (Taiwan) 11, 37–84.

Tsao, S., Li, T.C., Tien, J.L., Chen, C.H., Liu, T.K., Chen, C.H., 1992. Illite crystallinity and fission-track ages along the east Central Cross-Island Highway of Taiwan. Acta Geol. Tawain. 30, 65–94.

Van Avendonk, H.J.A., McIntosh, Kirk D., Kuo-Chen, H., Lavier, L.L., Okaya, D.A., Wu, F.T., Wang, C.Y., Lee, C.S., Liu, C.S., 2016. A lithospheric profile across northern Taiwan: from arc-continent collision to extension. Geophys. J. Int. 204 (1), 331–346. https://doi.org/10.1093/gji/ggv468.

Webb, A.A.G., 2013. Preliminary balanced palinspastic reconstruction of Cenozoic deformation across the Himachal Himalaya (northwestern India). Geosphere 9 (3), 572–587. https://doi.org/10.1130/GES00787.1.

Yu, S.B., Cheng, H.Y., Kuo, L.C., 1997. Velocity field of GPS stations in the Taiwan area. Tectonophysics 274, 41–59. https://doi.org/10.1016/S0040-1951(96)00297-1.